Int. J. Electrochem. Sci., 8 **(2013)** 274 - 289

International Journal of
ELECTROCHEMICAL
SCIENCE
www.electrochemsci.org

Determination of the Spatial Distribution of the Turbulent Intensity and Velocity Field in an Electrochemical Reactor by CFD

S.A. Martínez-Delgadillo[1,*], *J. Ramírez-Muñoz*[2], *H.R. Mollinedo P.*[3], *V.Mendoza-Escamilla*[4], *C.Gutiérrez-Torres*[5] *and J.Jiménez-Bernal*[5]

[1] Depto. Ciencias Básicas. Universidad Autónoma Metropolitana Azcapotzalco. Av. San Pablo 180. Azcapotzalco. CP 07740, México D.F. México.
[2] Depto. Energía, Universidad Autónoma Metropolitana Azcapotzalco. Av. San Pablo 180. Azcapotzalco. CP 07740, México D.F. México
[3] UPIITA, Instituto Politécnico Nacional. Av.IPN 2580, Ticoman. México D.F.
[4] Depto. Electrónica. Universidad Autónoma Metropolitana –Azcapotzalco. Av. San Pablo 180. Azcapotzalco. CP 07740, México D.F. México.
[5] LABINTHAP-SEPI. ESIME, Instituto Politécnico Nacional. U. P. Adolfo López Mateos. México D.F.
[*]E-mail: samd@correo.azc.uam.mx.

Received: 2 August 2012 / *Accepted:* 14 October 2012 / *Published:* 1 January 2013

CFD simulations of a rotating reactor used to remove hexavalent chromium (Cr(VI)) from industrial wastewaters are presented in this work. The reaction time dependence on the angular speed was experimentally demonstrated and these results were examined using the flow velocity and turbulence intensity fields obtained by computational fluid dynamics (CFD) simulations. It was found out that the flow velocity field and turbulence intensity are not homogeneous inside the reactor. Moreover, the increase in the electrodes rotational speed has no important effect in the turbulence intensity and velocity field inside the ring electrodes zone, which helps explaining why the reaction time is not decreased in the same proportion of angular speed increment. The study provides reference aids for optimization of impeller design and operation parameters.

Keywords: electrochemical reactor, CFD, turbulence, chromium hexavalent, wastewater.

1. INTRODUCTION

Mechanically, stirred tanks are employed for a large variety of applications in industrial processing like facilitation of chemical reactions in liquids, blending of miscible liquids, liquid-liquid

dispersion of immiscible liquids, solids suspension, and others. Several parameters that depict hydrodynamic behavior are traditionally used to evaluate the overall mixing process in stirred tanks. Among these, the flow velocity field discharged from an impeller and the turbulence intensity as function of the agitation rate and distance from the impeller. They are frequently used in practice, even in cases when the local turbulence is not isotropic [1]. In the flow velocity induced by the impeller, macromixing is driven by the largest scales of motion in the fluid [1,2], meanwhile, the distribution of turbulence intensity in the vessel is a measured of the mixing on smaller scales or micro-mixing, in which momentum diffusion due to turbulent velocity fluctuations -superposed on the principal motion- provides the final blending [2,3].

In this paper, we present a study of the hydrodynamic performance of an electrochemical reactor used in the treatment of wastewater contaminated with hexavalent chromium. Cr(VI) is one of the most hazardous pollutants discharged into the wastewaters by the electroplating industry and other manufacturing plants [4]. Cr(VI) is recognized as 1000 times more toxic than Cr(III), and therefore hazardous to human health. Additionally, wastewaters containing Cr(VI) are groundwater contamination sources. Therefore, this metal must be removed to reach acceptable concentration level (less than 0.1mg/L) and comply with the environmental regulations for wastewater disposal [5]. Although several methods can be used to remove Cr(VI) from water, in this work the use of a electrochemical treatment, based on the reduction of Cr(VI) to Cr(III), mainly by releasing ferrous ions (Fe (II)), from the anode into the solution when a direct electrical current is applied to an iron sacrificial anode is analyzed. By this method a 99.9 % removal of Cr(VI) can be achieved. The reaction 1, shows the Cr(VI) reduction into the solution.

$$6Fe^{2+}_{(aq)} + Cr_2O_7^{2-}{}_{(aq)} + 14\ H^{+}_{(aq)} \rightarrow 6Fe^{3+}_{(aq)} + 2Cr^{3+}_{(aq)} + 7\ H_2O(l) \qquad (1)$$

As seen, in reaction 1 the Cr(VI), is reduced to Cr(III) and the Fe(II) is oxidized to Fe(III), then the trivalent iron and chromium, can be precipitated and removed from the aqueous media. Treated water can be reused as rinsing water and the precipitate can be treated to separate the Cr(III) from the Fe(III), and then both can be reused as well. Therefore, the electrochemical method is a potential clean technology. However, during the process, an oxide fouling film is formed on the electrodes surface (passivation effect) in electrochemical reactors with no liquid mixing or static electrodes because of the poor diffusion and mass transfer, reducing the process efficiency and increasing the energy consumption [6]. Based on these effects, in this work the performance of an electrochemical reactor with rotating iron electrodes at different rotating electrode speeds was evaluated [7]. This electrochemical reactor had a stirred tank configuration of a cylindrical geometry with four standard baffles equally spaced disposed to prevent a swirl motion and tangential flow pattern of the mass fluid.

The impellers are in this case an arrangement of rotational rings joined by three flat blades, also serving as electrodes. The motion of the rings has a self-cleaning effect reducing fouling and increasing mass transfer efficiency due to high shear stress at the electrodes surface. However it was obtained that there was no important difference in the treatment time to reduce the Cr(VI) to Cr(III), when the rotating electrode speed was increased. In that work [7], it was partially demonstrated that the average turbulent intensity had a reduced increment value by only 0.2%, when rotating electrode

speed was increased from 150 rpm to 200 rpm. In this type of reactors, tank baffles are required to establish the appropriate flow pattern to promote positive top-to-bottom turnover (macromixing), reducing blend time. In addition, the turbulence intensity is the primary responsible for micromixing or eddy diffusion of momentum, heat and mass [8]. Therefore, micromixing is the limiting step in the progress of fast reactions. From the above discussions, it is apparent that the performance of a stirred tank reactor depends largely on the characteristics of pattern flow and turbulent intensity generated by an impeller. For this reason, several works have been focused on identifying the hydrodynamical characteristics of the flow induced by basic impeller types and its relationship with the most important design parameters like impeller off-bottom distance, impeller diameter relative to the tank diameter, liquid depth, spacing between impellers, aspect ratio of the vessel, tank bottom, size and shape of baffles [9-17]. For this purpose, numerical and experimental studies have been carried out to establish the design and operating parameters needed to enhance the performance of such reactors. Knowing the characteristics of turbulent flow and its properties can be very useful for designing a stirred tank, scale up the process, and evaluate energy consumption and control of product quality. However, experimental techniques for the acquisition of experimental data are generally expensive due to the unstable nature of turbulent flows, the complexity of the geometry of the impeller blade, and the relative movement between the elements of the fluid [18]. CFD can be used to simulate turbulent flows in stirred tank electrochemical reactors and are useful for predicting the hydrodynamic behavior of the reactor [19]. Then, it is possible to determine different characteristics as the velocity field, the vorticity, turbulent intensities, and circulation patterns, among others. Due to the high computing capacity available in current computers, numerical tools such as CFD have reached a considerable development, allowing great advances in process simulation in fluid media. CFD modeling cannot completely replace experimentation, but it has become a useful tool, which complements and improves the experimental work [20, 21]. In this work, more detailed evaluations were performed to get better understanding of the performance inside the electrochemical reactor, because other parameters as velocity magnitude, velocity magnitude, x-velocity and tracer concentration were evaluated and correlated with the turbulent intensity at different positions, inside and outer the rotating ring electrodes at different angular velocities.

2. MATERIALS AND METHODS

Tests were performed in an electrochemical batch reactor with a synthetic wastewater prepared with potassium dichromate. The viscosity (μ) and density (ρ) of the process fluid were 1.0019×10^{-3} Pa-s and 998 kg/m^3, respectively. The electrochemical reactor capacity was 8.5 liters. To produce turbulence in the reactor, a rotating iron ring electrode was used during the electrochemical chromium removal process. The rotating iron electrodes contained 14 iron steel rings allocated in a sequence of one cathode followed by one anode and separated 1.0 cm from each other. Each ring has a diameter of 11.5 cm, 7 rings function as cathodes and the other 7 as anodes. The liquid height was 24.6 cm and the tank diameter was 21.5 cm. The superficial area of each iron ring was 75.0 cm^2. A shaft connected to a variable speed motor was used to support the ring arrangement and to control the electrode revolutions

per minute (rpm).The tests were performed in the turbulent range: 75 rpm (*Re*=16,470), 150 rpm (*Re*=32,940) and 230 rpm (*Re*=50,509) rpm. Where $Re=\rho d^2 N/\mu$ is Reynolds number and *N* the electrode rotational speed in revolutions per second. A constant electric current of 5.0 amperes was applied during the process, using a direct current power supply. Figure 1 shows the configuration of the stirred tank electrochemical reactor.

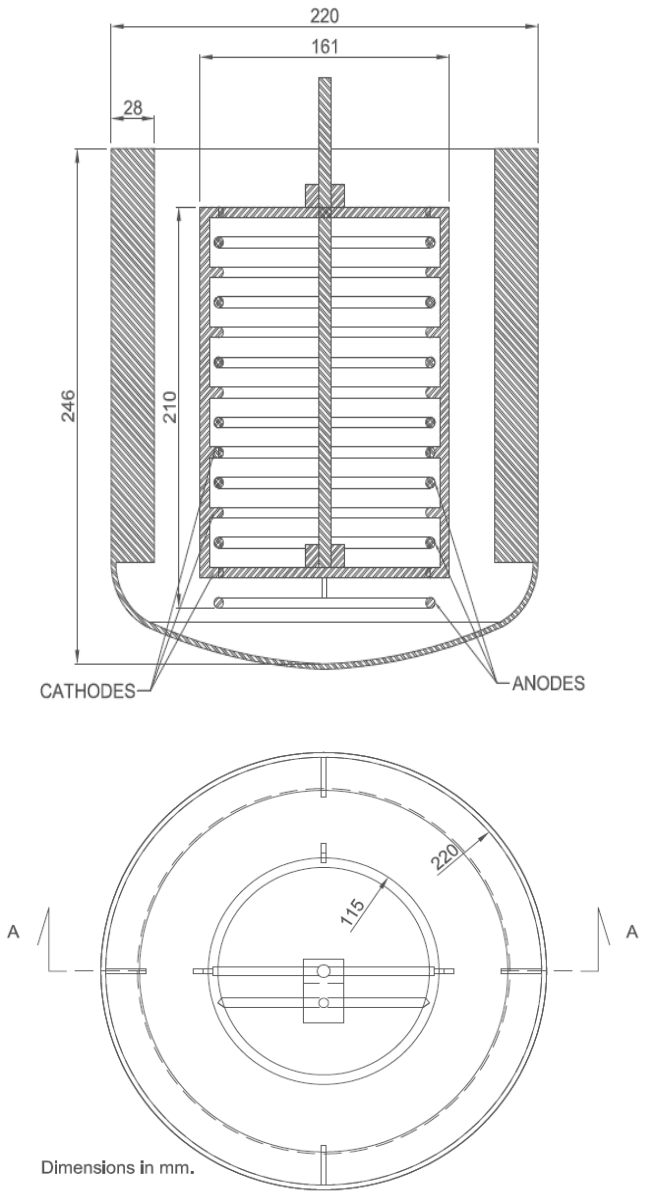

Figure 1. Configuration of stirred tank electrochemical reactor.

The related CFD model of the reactor was prepared to analyze the performance of the reactor at different steady state operational angular velocities: 75, 150 and 230 rpm. The reactor model was meshed using 1,547,617 tetrahedral cells. Figure 2, shows the mesh used for the electrochemical reactor.

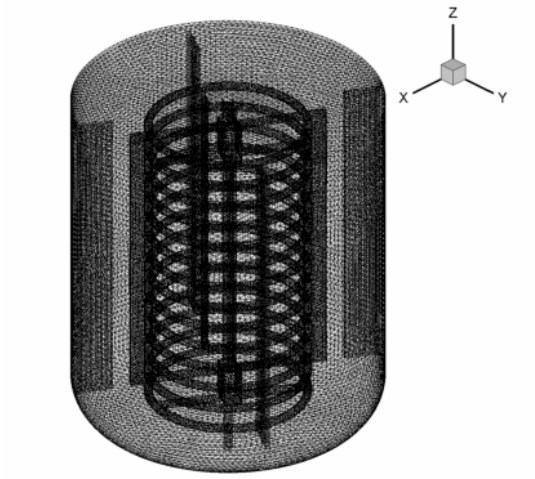

Figure 2. Electrochemical reactor mesh.

The reactor was modeled using a single rotational reference frame with a steady rotational speed. The rotational system of ring electrodes and impellers were assumed as a moving wall (with no slip condition) attached to the moving reference frame; the whole surfaces of the vessel including the baffles of the reactor were considered as stationary wall boundary condition. The conservation equations were set to a rotating reference system, expressing the governing equations of fluid flow for a steadily rotating frame in terms of the relative velocity $\vec{v}_r$. The steady state continuity equation (mass conservation) for incompressible fluid can be written as follows:

$$\nabla \cdot \vec{v}_r = 0 \qquad (2)$$

where: $\overrightarrow{v_r}$ = relative velocity vector.

The conservation of momentum for a rotating reference frame is given by:

$$\frac{\partial}{\partial t}\left(\rho \vec{v}_r\right) + \nabla \cdot \left(\rho \vec{v}_r \vec{v}_r\right) + \rho\left(2\vec{\omega} \times \vec{v}_r + \vec{\omega} \times \vec{\omega} \times \vec{r}\right) = -\nabla p + \nabla \cdot \left(\bar{\tau}\right) + \rho \vec{g} + \vec{F} \qquad (3)$$

Where: τ= viscous stress tensor, ρg= gravitational body force and $\vec{F}$ = external force vector. The momentum equation contains two additional acceleration terms: the Coriolis acceleration, and the centripetal acceleration. A pressure-based segregated algorithm solver has been used, where the governing equations are solved sequentially. For the pressure–velocity coupling the semi-implicit pressure-linked equation (SIMPLE) algorithm was used, the Standard scheme was selected for pressure discretization, and for the momentum discretization, the first order upwind scheme was used in the initial solution and second order for the final solution. The realizable κ-ε turbulent model was used because presented better results than standard and RNG models. The CFD simulations were performed using the commercial software Fluent, 6.3.26. Due to the unsymmetrical configuration of the blades, a complete three dimensional model reactor was used. Different parameters such as

velocity magnitude, x velocity, turbulent intensity and tracer concentration were evaluated for different positions (indicated in figure 3), at different angular velocities, as shown in table 1a and 1b.

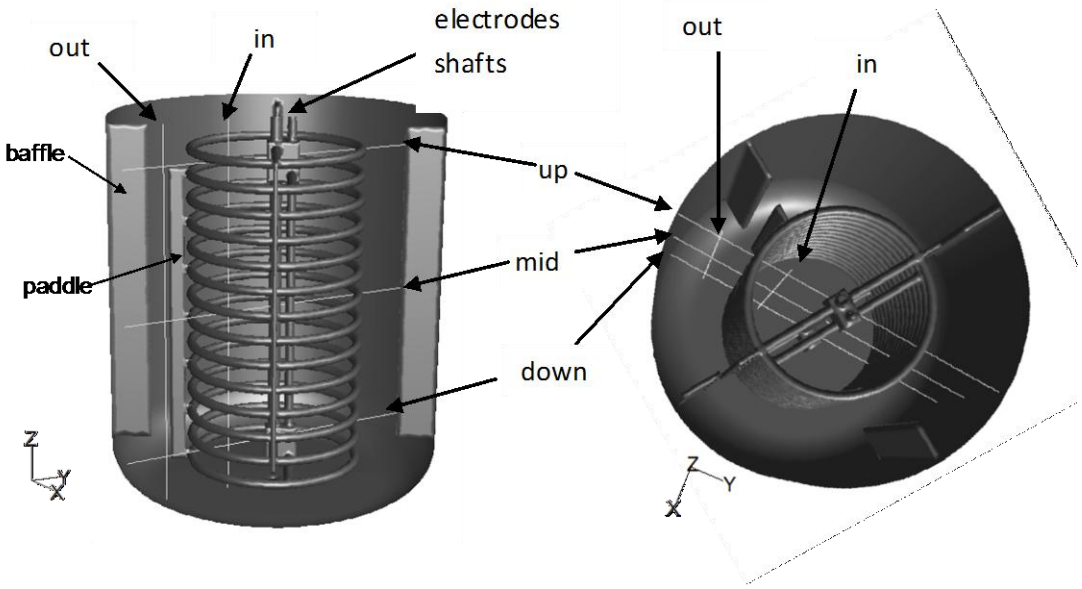

Figure 3. Positions in the electrochemical reactor where different parameters were evaluated.

Table 1a. Coordinates in the electrochemical reactor for the up, mid and down positions, where different parameters were evaluated.

	position					
coordinate	*up*		*mid*		*down*	
X	0	0	0	0	0	0
Y	-0.1075	0.1075	-0.1075	0.1075	-0.1075	0.1075
Z	0.22	0.22	0.121	0.121	0.03	0.03

Table 1b. Coordinates in the electrochemical reactor for the in and out positions, where different parameters were evaluated.

	position			
coordinate	*in*		*out*	
X	0	0	0	0
Y	-0.035	-0.035	-0.08	-0.08
Z	0	0.246	0	0.246

In the case of the tracer tests, a flow electrochemical reactor was evaluated and a tracer with the same properties as the water was simulated. The tracer concentration was homogeneous throughout the reactor at the beginning of the test. Then, water was fed in the reactor at velocity magnitude of 1 m/s,

based on the inlet projected area (3.227e-05 $m^{2)}$. The tracer was removed gradually from the reactor due to the entering water and its concentration also was evaluated at the reactor exit.

3. RESULTS AND DISCUSSION

Table 2 shows experimental results obtained of chromium concentrations reduction from 130 mg/L to less than 0.5 mg/L, at different angular velocities (rpm).

Table 2. Concentration reduction time for different angular velocities.

Angular velocity [rpm]	Reaction time [min]
0 (theoretical)	38
0	42
75	30
150	24
230	22

The theoretical time of the process was calculated considering that reaction (1) was instantaneous and the Cr (VI) is reduced to Cr (III), only by the anodically generated Fe^{2+} [22]. The increase of angular velocity in the reactor does not have a linear effect on the concentration reduction time as it is observed from table 1. When the total reaction time experimental values are compared it is found a reaction time reduction of 29% when angular velocity goes from 0 rpm to 75 rpm. If the angular velocity is doubled (from 75 rpm to 150 rpm), the reaction time reduction reaches about 20%. Finally, a 53% increase in angular velocity (150 rpm to 230 rpm), the reaction time reduction only adds up to 8.3%. As discussed above, one of the main characteristics of turbulence is that it enhances mass transfer when it is present in a flow field. The fluid motion sets up the concentration distribution within the reactor, which in turn influences the reaction rate [1], and the turbulence intensity ensures a fast mixing on smaller scales [1, 2]. Bakker [23] carried out gas–liquid simulations with fermenter, equipped with a radial impeller at the bottom and three axial impellers at the top, incorporating models for gas dispersion, bubble coalescence and breakup, and inter-phase mass transfer. They found that the mass transfer coefficient is highest near the impellers, i.e. where the turbulence intensity is highest. The effects of turbulent increasing mass transfer rates have also been observed in external flows around cylinders [24] where a direct correlation between increments in turbulent intensity values and mass transfer was reported, and stirred tanks [25] where the mass transfer increase was reported to depend on angular velocity. To evaluate the modifications induced on the flow once the angular velocity is increased, turbulent intensity is evaluated for 75 rpm, 150 rpm and 230 rpm. Turbulent Intensity is defined for each velocity component as the root mean square of the velocity fluctuations

referenced to a characteristic mean flow velocity U_o. For the x velocity component, it is given in equation 4.

$$\boldsymbol{T_x} = \frac{\left(\overline{\boldsymbol{u_1' u_1'}}\right)^{\mathbf{1/2}}}{\boldsymbol{U_0}} \qquad (4)$$

Where $\boldsymbol{T_x}$ is the turbulent intensity in the streamwise direction, U_0 is the average velocity, u_1' is the streamwise fluctuating velocity component. The overall turbulent intensity is defined as the average of $\boldsymbol{T_x}$, $\boldsymbol{T_y}$, and $\boldsymbol{T_z}$, as shown in equation 5.

$$\boldsymbol{T} = \frac{\left(\frac{\mathbf{1}}{\mathbf{3}}\overline{u_i' u_i'}\right)^{1/2}}{U_0} \qquad (5)$$

Since the flow inside the reactor was numerically simulated. Figure 3a shows a complete 3-D distribution of turbulent intensity for an angular velocity of 230 rpm.

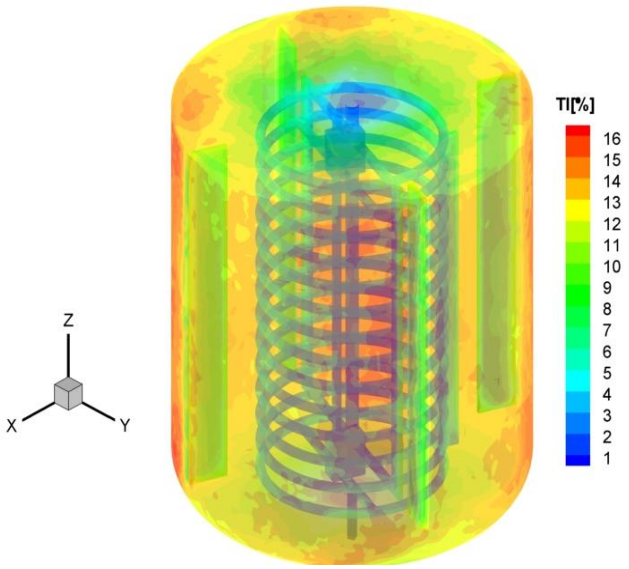

Figure 3a. Three dimensional distribution of turbulent intensity (230 rpm).

As seen, although this image is illustrative of the turbulent intensity distribution within the reactor, it is difficult to analyze the spatial distribution of turbulent intensity along the three coordinate axes and the influence of the ring location on the flow field. To analyze spatial location influence on the turbulent intensity values, turbulent intensity distribution at five different locations (shown in table 1a and 1b, and figure 3), along the z-axis (figures 4) and y-axis (figure 5), are presented.

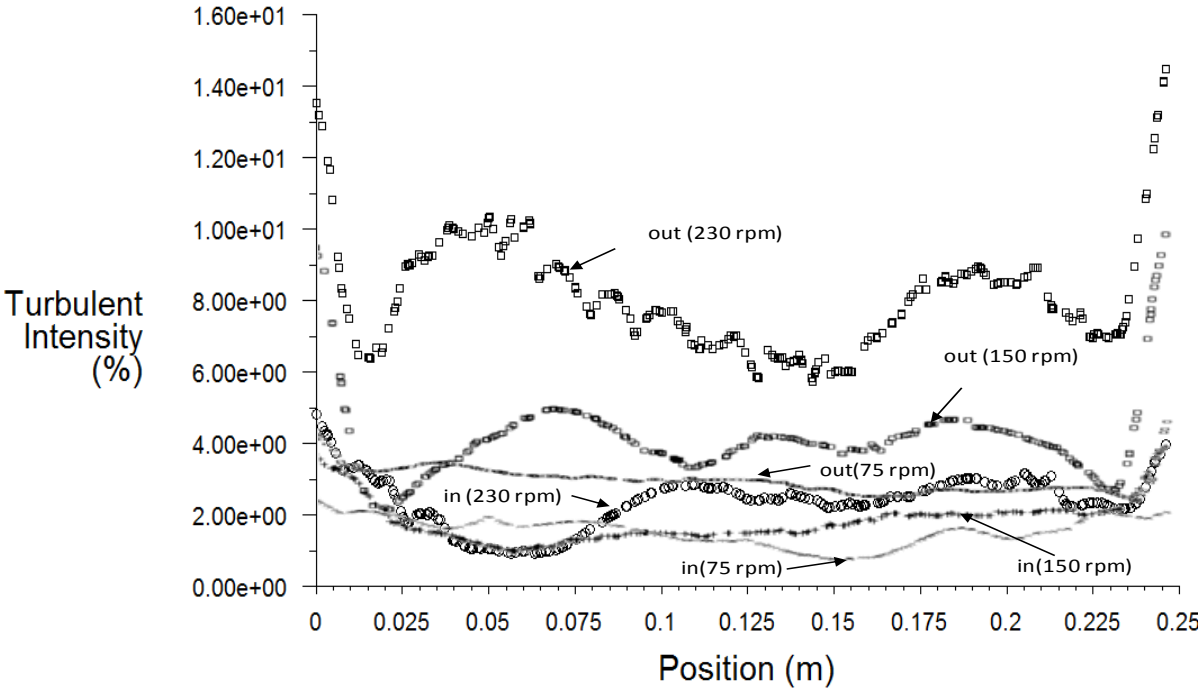

Figure 4. Turbulent intensity along the z-axis for the reactor operated at 75, 150 and 230 rpm.

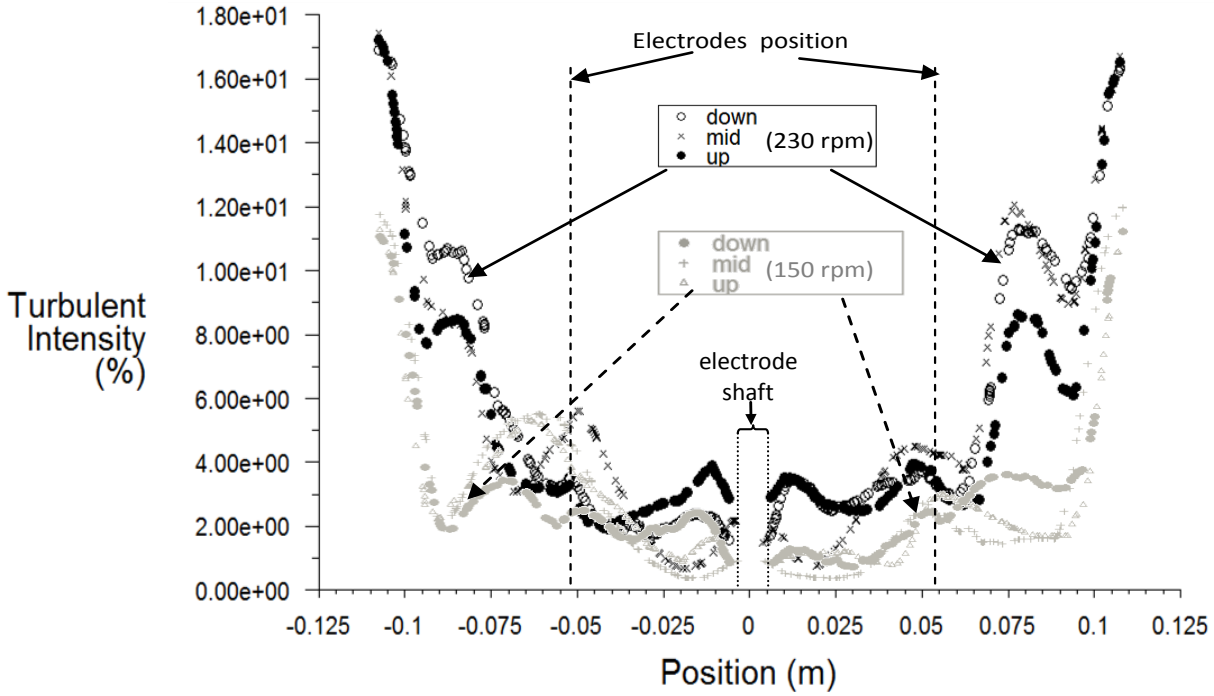

Figure 5. Turbulent intensity along the y-axis for *down*, *mid* and *up* positions, in the reactor operated at 150 and 230 rpm.

As shown, the highest turbulent intensity (TI) is reached at the 230 rpm, but in the *out* position (outside the ring electrodes). In general, at the three angular velocities, higher TI values at the *out* position are reached. However, lower TI values are reached at the *in* position (inside the ring electrodes zone). Moreover, the TI values at the *in* positions are similar for 230 rpm and 150 rpm. In

figure 5, the TI values for both rpms along the y-axis at *down*, *mid* and *up* positions in the electrochemical reactor are presented. As shown, turbulent intensity grows in the radial direction (here represented by the y coordinate). It increases up to an inflection point located next to y = 0.05 m and y = -0.05 m, zone limited by the electrodes position lines, which is approximately the ring electrodes diameter. However, the TI values inside the ring electrodes zone are similar for both angular velocities. On the other hand, the TI values out of this zone are higher at 230 rpm than at 150 rpm.

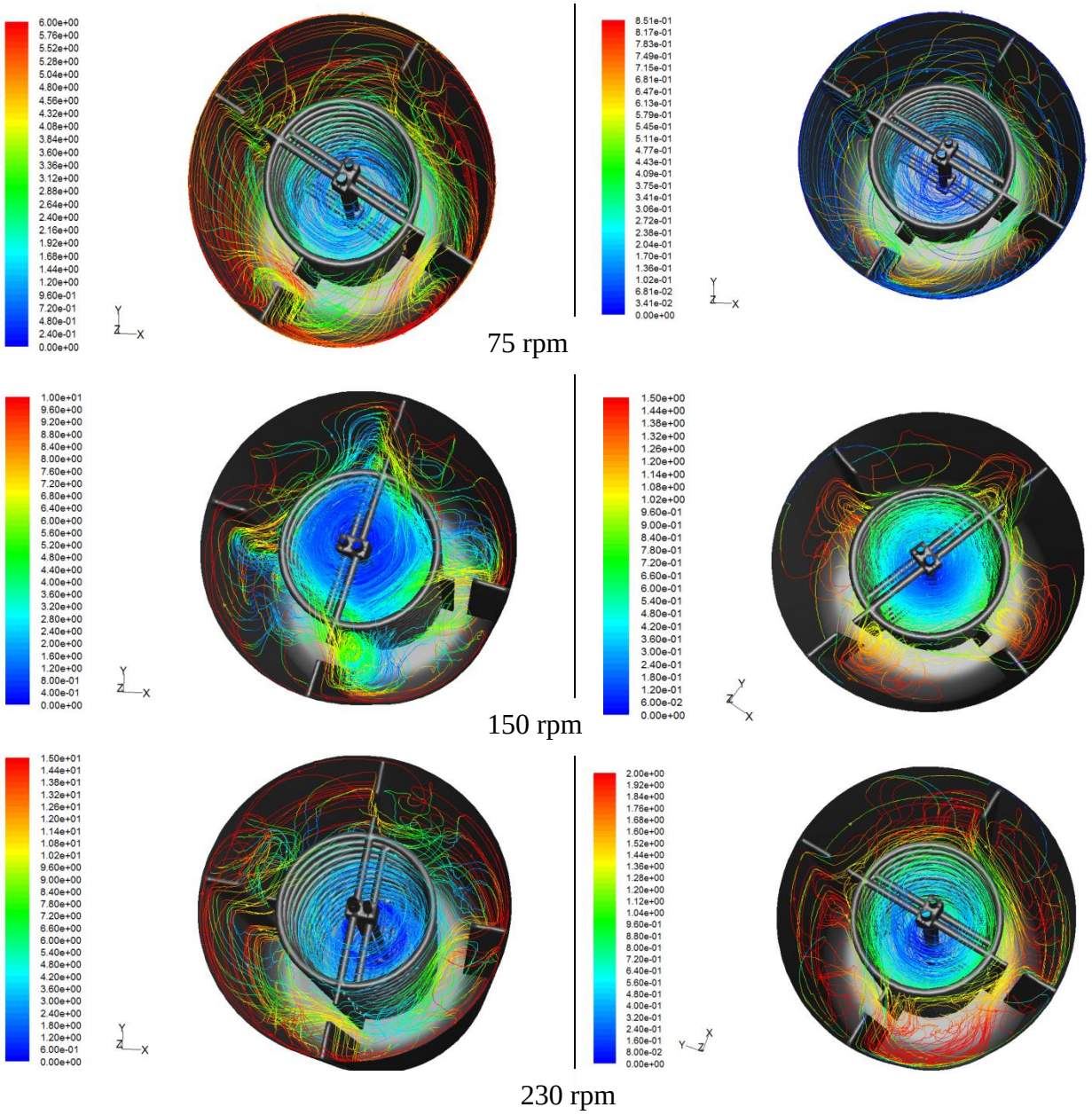

Figure 6. Pathlines colored by a) turbulent intensity and b) velocity magnitude in the electrochemical reactor operated at 75, 150 and 230 rpm.

The maximum values for turbulent intensity are always reached near the tank wall, as seen in figure 6a. These are the critical points were turbulent intensity is mainly increased, and therefore the mass transfer is increased. In the same figure, it is possible to see that also higher TI zones are produced between the baffles and the electrode paddles. On the other hand, the lowest TI values are located in the zone inside the ring electrodes at all angular velocities. Figure 6b, shows the pathlines colored by velocity magnitude for each angular velocity in the electrochemical reactor. As seen, the lowest velocity magnitude values are reached at 75 rpm and for all the rpm, there are lower values of velocity magnitude and TI, in the zone inside the ring electrodes.

In the outer zone (between the reactor wall and the outer ring electrodes wall), higher velocity magnitude are generated.

Figure 7, shows the velocity magnitude values along the y-axis at for *down*, *mid* and *up* positions, in the reactor operated at 75, 150 and 230 rpm.

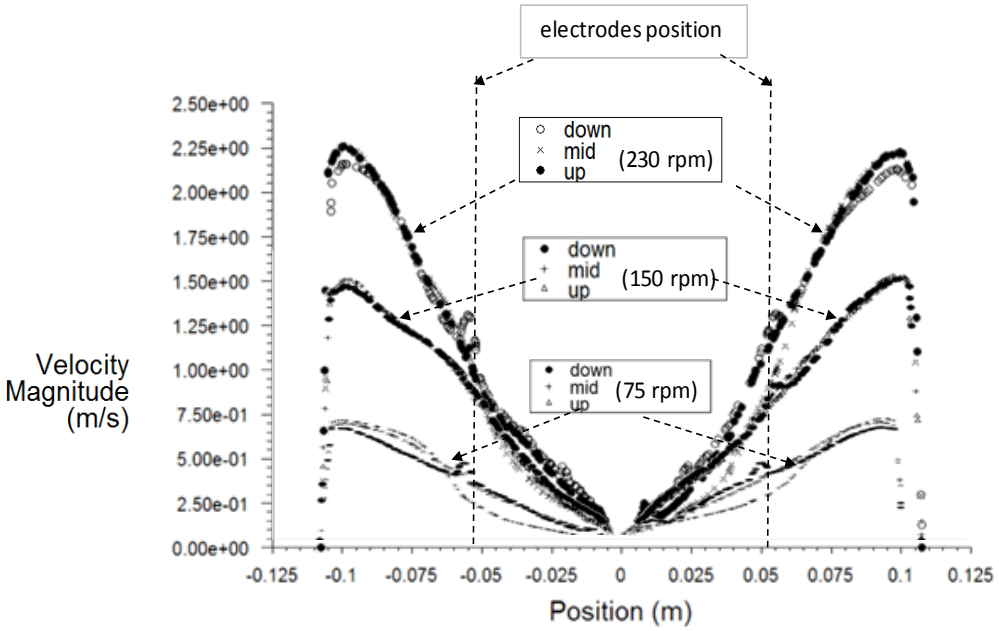

Figure 7. Velocity magnitude values along the y-axis at *down*, *mid* and *up* positions, in the reactor operated at 75, 150 and 230 rpm.

As shown in these figures, the velocity magnitude drops quickly as one moves towards the electrodes centerline and corroborate that the lowest velocities are reached inside the ring electrodes. An important fact is that for 150 and 230 rpm, the velocity magnitude values are similar inside the ring electrodes, but at the outer zone higher velocities corresponds to higher rpm.

In addition, figure 8 shows that along the reactor the velocity magnitude values inside (*in* position) the ring electrodes are very similar in both angular velocities.

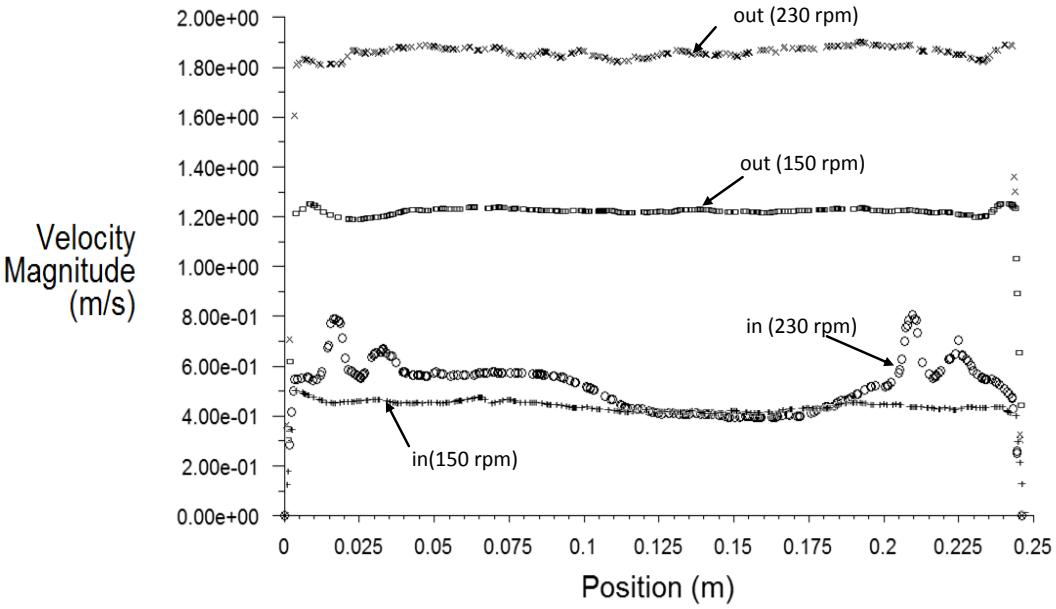

Figure 8. Velocity magnitude along the z-axis at for *in* and *out* positions, in the reactor operated at 150 and 230 rpm.

The zone inside the ring electrodes is about 35% of the reactor volume and it has similar behavior at both ring electrodes rotational speed, 150 rpm and 230 rpm. Therefore, increasing the rotational speed has no important effects in this zone and consequently, in the time Cr(VI) reduction electrochemical process.

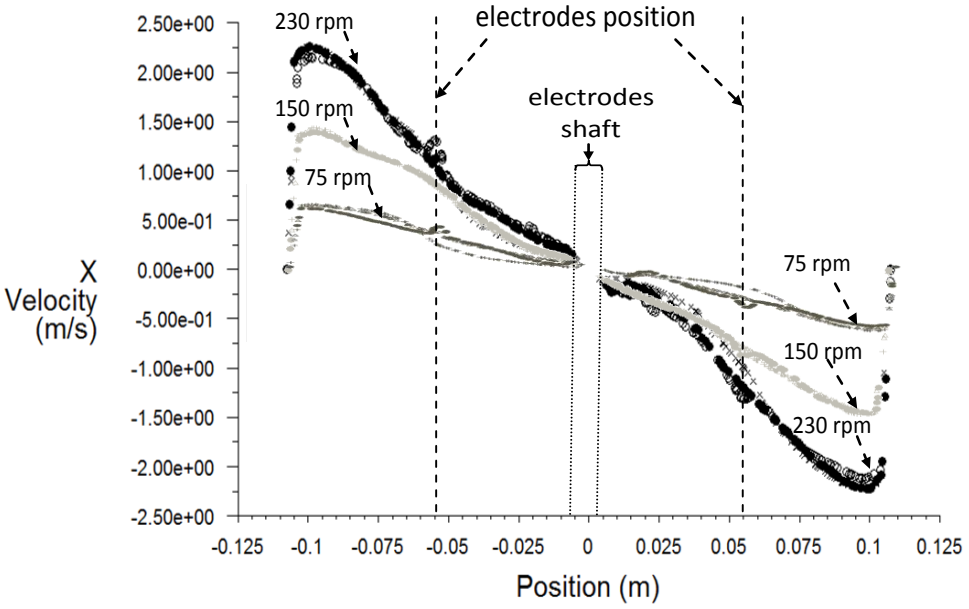

Figure 9. Velocity values along the x-axis at *down*, *mid* and *up* positions, in the reactor operated at 75, 150 and 230 rpm

The reactants Fe(II) an Cr(VI) ions must be transported to the highest turbulence intensity zone located outer of the ring electrodes zone to increase the reaction rate. Considering that this effect has an important impact in the time electrochemical process, the x-velocity was evaluated at the different positions inside the reactor for all the three angular velocities, because the reactants Fe(II) an Cr(VI) ions are transported to the outer ring electrodes zone and this effect has an important impact in the time electrochemical process.

Figure 9, shows that at 150 rpm and 230 rpm the x-velocity is higher than at 75 rpm, making faster the reduction of the Cr(VI), but in the zone inside the ring electrodes, the fluid x-velocity is again very similar, as in the case of TI and velocity magnitude, as was shown before. The tracer tests performed at150 rpm and 230 rpm, confirm that for both cases, the tracer stills trapped inside the rings zone, it only rotates without an efficient mixing, as shown in figure 10. In addition, it can be observed that near the baffles (*mid* and *up* positions), in the opposite direction of the fluid movement, there are zones with higher tracer concentration due to the low velocity in those areas.

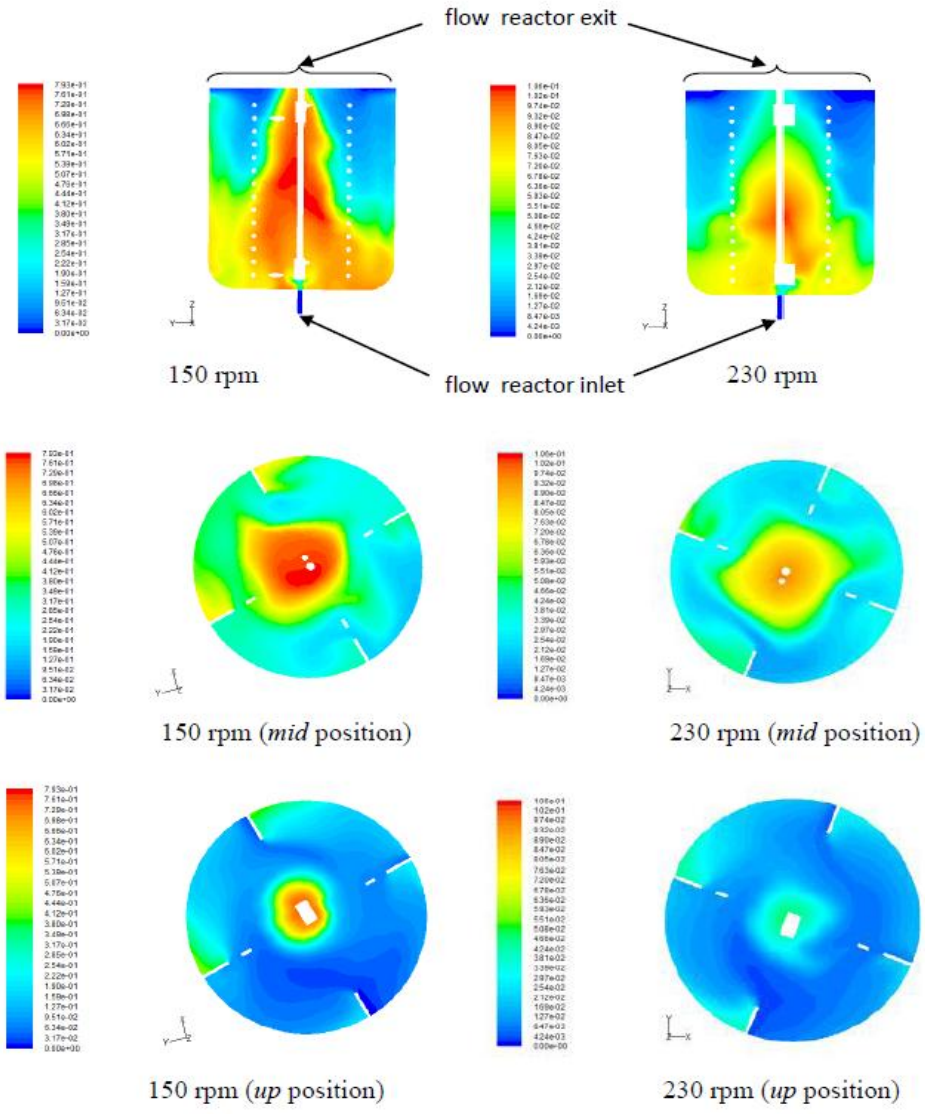

Figure 10. Contours of tracer concentration in the flow reactor at 150 and 230 rpm.

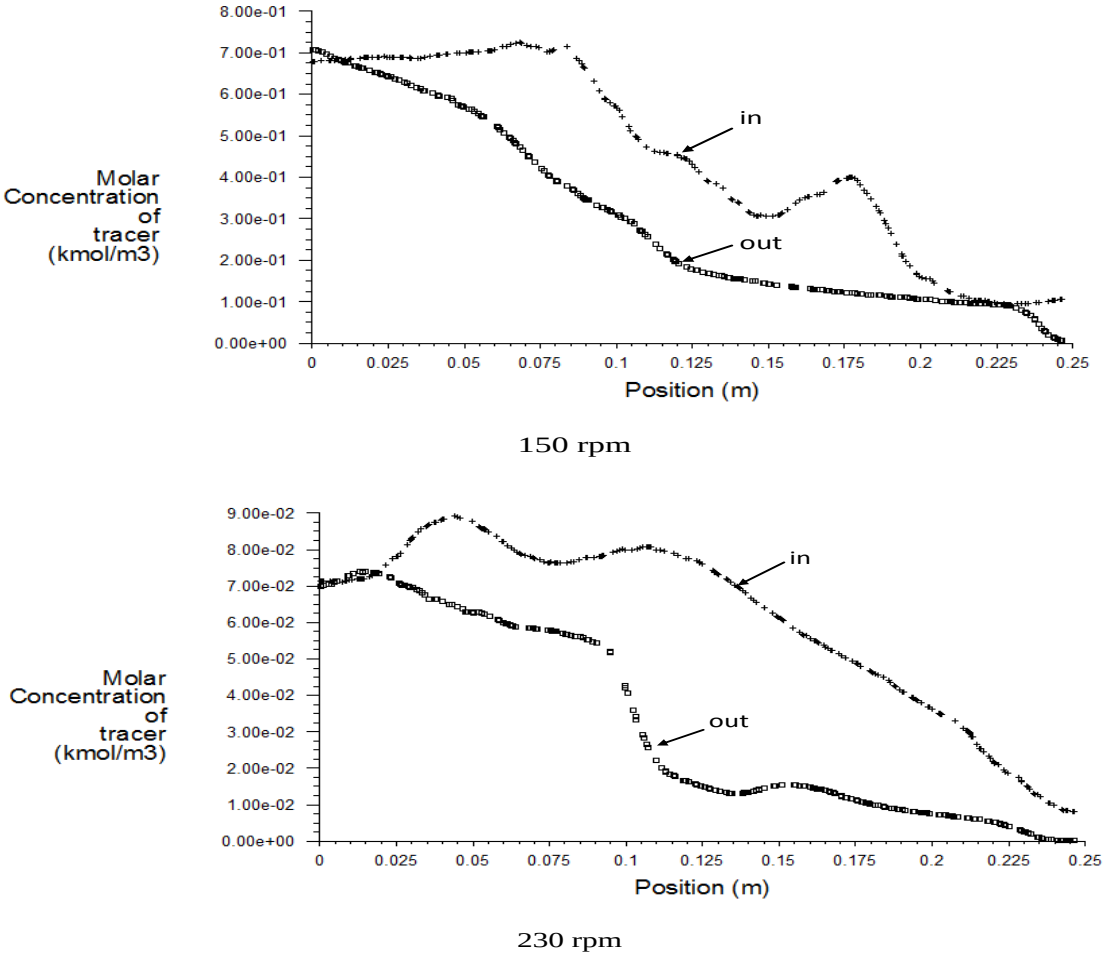

Figure 11. Tracer concentration in the flow reactor at the in and out positions operated at 150 rpm and 230 rpm.

Figure 11, shows that at both rpm, the tracer concentration along the electrochemical reactor. As seen, inside the rings (*in* position) the concentration is higher than in the exterior zone (*out* position) because the lower velocity and turbulence in this zone. As shown in figure 12, this effect produces that at the reactor exit the tracer concentration is higher in the central part.

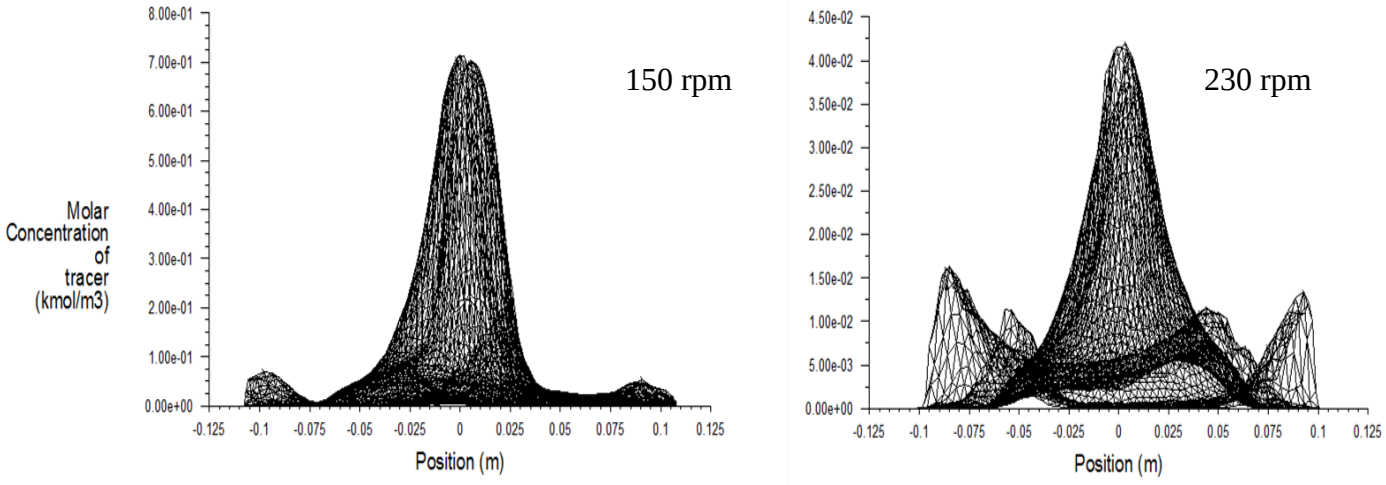

Figure 12. Tracer concentration in the flow reactor at the reactor exit for 150 rpm and 230 rpm.

The results showed that at both angular velocities, 150 rpm and 230 rpm, the behavior is similar and the mixing is deficient. These effects limited the transport of reactants, and then the Cr(VI) reduction rate, no matter the angular velocity were increased. Because an important fraction of volume has similar behavior at 150 rpm and 230 rpm, the reactants transport throughout the reactor is limited, and then increasing the agitation rate form 150 rpm to 230rpm, has no important effect in the Cr(VI) time reduction. In this case, both, the top-to-bottom turnover flow and the turbulence intensity could be increased putting axial-flow impellers (e.g. pitched blade impellers) inside the ring electrodes. According to these results, the current configuration of the electrochemical reactor, mainly the rotating ring electrodes must be changed to improve its overall mixing performance and reduce the energy consumption.

4. CONCLUSIONS

Increasing angular velocity of the rotating ring electrode will increase magnitude velocity and the turbulent intensity that hence mass transfer, especially outside the ring electrodes. However, no important difference on the Cr(VI) reduction rate was obtained when the rpm of the ring electrodes was increased from 150rpm to 230 rpm. At both rpm, the magnitude velocity and the turbulent intensity behavior inside the rotating ring electrodes zones are very similar. Due to this effect, the transport of the reactants (i.e. Fe(II) and Cr(VI)) throughout the reactor was limited, causing that the increase in the rpm had no important outcome on the Cr(VI) reduction rate. Based on these results, it is necessary to change the electrodes configuration to improve the electrochemical performance and reduce the energy consumption. These results are very useful because different operational deficiencies in the electrochemical reactor were found and possible improvements can be suggested. These results also show the usefulness of CFD simulations to have better understanding of the reactor operation.

ACKNOWLEDGEMENTS
Financial supports of this work by the Consejo Nacional de Ciencia y Tecnología (I010/176/2012) are gratefully acknowledged.

References

1. J. M. Oldshue. Fluid mixing technology. McGraw-Hill Publications Co., New York, N. Y., 1983.
2. E. L. Paul, V. A. Atiemo-Obeng, S. M. Kresta. HANDBOOK OF INDUSTRIAL MIXING SCIENCE AND PRACTICE. Wiley Interscience, 2004.
3. H. Schilichting. Boundary-Layer Theory. McGraw-Hill Inc. 1968.
4. L. Liu, X. Ma. *J. Cleaner Prod.* 18 (2010) 1731.
5. SEMARNAP, 1997. Nom-001-Ecol-1996, Diario Oficial de la Federación, México, 1997. (In Spanish).
6. S. A. Martinez, M.G. Rodriguez, C. Barrera. *Water Sci. Technol*. 42 (2000) 55.
7. S. A. Martínez-Delgadillo, H. R. Mollinedo-Ponce, V. X. Mendoza-Escamilla, C. Gutierrez-Torres,

J. Jimenez-Bernal, C. Barrera-Diaz. *J. Cleaner Prod.* 34 (2012) 120.
8. Masoud Rahim, Saeideh Amraei, and Ammar Abdulaziz Alsairafi. *Korean J. Chem. Eng.*, 28(6) (2011) 1372.
9. J. Bertrand, J.P. Couderc, H. Angelino. *Chem. Eng. Sci.* 35 (1980) 2157.
10. J. Costes, J.P. Couderc. *Chem. Eng. Sci.* 43 (1988) 2751.
11. S. M. Kresta, P. E. Wood. *Can. J. Chem Eng*. 71 (1993) 42.
12. A.W. Nienow. *Chem. Eng. Sci.* 52, (1997) 2557.
13. V. P. Mishra, K. N. Dyster, A. W. Nienow, J. Mckemmie, Z. Jaworski. *Can. J. Chem Eng*. 76 (1998) 577.
14. Z. Jaworski, K. N. Dyster and A. W. Nienow. *Trans IChemE*. 79, (2001) Part A.
15. Y. B. Wu and W. Feng . *Proceedings of the Fifth International Conference on Fluid Mechanics,* DOI: 10.1007/978-3-540-75995-9 *(*2007) 138.
16. S. Roya, S. Acharya, M. D. Cloeter. *Chem. Eng. Sci.* 65, (2010) 3009.
17. H. Singh, D. F. Fletcher, J. J. Nijdam. *Chem. Eng. Sci.* 66 (2011) 5976.
18. M. Ammar, Z. Driss , W. Chtourou, M. S. Abid. *Cent. Eur. J. Eng*. 1(4) (2011) 401.
19. R. Thilakavathi, D. Rajasekhar, N.Balasubramanian, C. Srinivasakannan, A. A. Shoaibi. *Int. J. Electrochem. Sci.*, 7 (2012) 1386.
20. M.H. Vakili, M. Nasr Esfahany. *Chem. Eng. Sci.* 64 (2009) 351.
21. J. Derksen. *Flow Turbul. Combust*. 69 (2002) 3.
22. Rodríguez, M.G., Aguilar, R., Soto, G., Martínez, S.A. *J. Chem. Technol. Biotechnol*. 78, (2003) 371.
23. Bakker, A. Ph.D. dissertation, Delft University of Technology, The Netherlands. 1992.
24. J. Kestin, R. T. Wood. J *Heat Trans-T ASME*. 93 (1971) 321.
25. W .J. N. Fernando, M.R. Othman and D.G.G.P.Karunaratne. *Int. J. of Eng.Tech.*. 11, February 2011.